




RESEARCH ARTICLE | JULY 31 2023

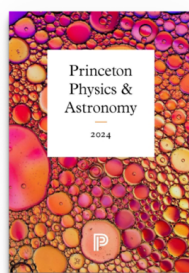
Nodal-line symmetry breaking induced colossal anomalous Hall and Nernst effects in Cu_2CoSn Heusler compound

Gaurav K. Shukla ; Ujjawal Modanwal; Sanjay Singh  



Appl. Phys. Lett. 123, 052402 (2023)

<https://doi.org/10.1063/5.0155940>



Browse our new Physics and Astronomy Catalog
30% off titles with code **P326**



Nodal-line symmetry breaking induced colossal anomalous Hall and Nernst effects in Cu_2CoSn Heusler compound

Cite as: Appl. Phys. Lett. **123**, 052402 (2023); doi: 10.1063/5.0155940

Submitted: 25 April 2023 · Accepted: 14 July 2023 ·

Published Online: 31 July 2023



View Online



Export Citation



CrossMark

Gaurav K. Shukla,  Ujjawal Modanwal, and Sanjay Singh^{a)} 

AFFILIATIONS

School of Materials Science and Technology, Indian Institute of Technology (Banaras Hindu University), Varanasi 221005, India

^{a)} Author to whom correspondence should be addressed: ssingh.mst@iitbhu.ac.in

ABSTRACT

The presence of topological band crossings near the Fermi energy is essential for the realization of large anomalous transport properties in the materials. The topological semimetals host such properties owing to their unique topological band structure, such as Weyl points or nodal lines (NLs), those are protected by certain symmetries of the crystal. When the NLs break out in the system, a large Berry curvature arises in the surrounding area of the gapped NL. In the present work, we studied anomalous transport properties of Cu_2CoSn compound, which has a cubic Heusler crystal structure (space group: $\text{Fm}\bar{3}\text{m}$). Cu_2CoSn full Heusler compound possesses NLs at the Fermi level that is protected by mirror reflection symmetries of the lattice. Upon introducing the spin-orbit coupling in the Hamiltonian and by setting the magnetization axis along the [001] direction, we found that the NLs are gapped out and large Berry curvature arises in the system. The integral of Berry curvature gives the intrinsic anomalous Hall conductivity (AHC) about 1003 S/cm and the anomalous Nernst conductivity (ANC) about 3.98 A/m K at the Fermi level. These values of AHC and ANC are comparable to the largest reported values for the Co_2MnGa Heusler compound. Therefore, Cu_2CoSn becomes a newborn member of the family of full Heusler compounds, which possesses giant AHC and ANC that can be useful for the spintronics application.

Published under an exclusive license by AIP Publishing. <https://doi.org/10.1063/5.0155940>

Anomalous Hall effect (AHE) describes the appearance of additional transverse voltage in the ferromagnetic materials induced by longitudinal charge flow even in the absence of external magnetic field.^{1–8} AHE originates from the interplay between spin-orbit coupling (SOC) and the magnetization of the material.^{1–4} AHE garnered significant research interest in condensed matter physics for its utilization in spintronic, Hall sensors and as a fundamental tool to detect the magnetization in a small volume, where the magnetometry measurements are not compatible.^{9–11} The origin of AHE attributed to the two mechanisms—extrinsic and intrinsic. The extrinsic mechanism is caused by defects, impurities, and scattering center within the material, while the intrinsic mechanism stems from Berry curvature linked to the electronic band structure, independent from any form of scattering.^{12–16} The Berry curvature is equivalent to the intrinsic pseudo-magnetic field in the reciprocal space, which leads to the transverse deflection of spin-polarized moving charge carriers and develops the intrinsic AHE.¹⁶ Anomalous Nernst effect (ANE), another interesting phenomenon that is a counterpart of AHE, describes the generation of transverse voltage drop in the material with broken TRS,

when subjected to a longitudinal temperature gradient.^{17–19} The ANE is closely analogous to the AHE, i.e., ANE also arises from intrinsic and extrinsic contributions.^{18,20} Several experimental and theoretical studies on ANE have been reported on magnetic materials.^{18,21–24}

The discovery of topological materials simulated significant interest in condensed matter physics for their unique electronic properties and potential for technological applications.^{25–28} Among these materials, topological semimetals (TSMs) have emerged as a particularly intriguing class of gapless electronic phases exhibiting topologically protected stable crossings of energy bands.^{25,26} The Dirac semimetal, a category of TSMs, exhibits a fourfold degeneracy at the Dirac point, while Weyl semimetals (WSMs), which are a subset of Dirac semimetals, arise when inversion and/or time-reversal symmetry (TRS) is broken, leading to the formation of Weyl points and the lifting of this degeneracy.^{29–32} WSMs show a variety of interesting phenomena, such as chiral anomaly, chiral magnetotransport, and anomalous transport response owing to their unique band topology.^{33–42} WSMs have been extensively discovered as a consequence of breaking inversion symmetry (IS).^{35–39} More recently, a new class of WSMs, known

as magnetic WSMs, have been identified arising from the breaking of time-reversal symmetry (TRS).^{40,41} The notable advantage of magnetic WSMs over conventional WSMs is their susceptibility to easy manipulation of band topology by controlling the direction of the magnetic moment.^{40,42} In addition to the zero dimension crossing of bands in the WSMs, the higher dimension crossing is also possible, where the bands cross each other along a closed curve called nodal lines (NLs).^{43,44} These NLs are generally protected by the certain symmetry of the crystal. For example, the TRS and IS can protect the NLs in the absence of spin-orbit coupling (SOC).^{45,46} The mirror symmetries with opposite eigenvalues can also protect the NLs in both the presence and absence of SOC.^{47–49}

WSMs are prominent materials for the large AHE and ANE as the Weyl points in the momentum space act as the magnetic monopole and are the source and drain of the Berry curvature.^{4,18} In addition to the Weyl points, if the NLs present in the k -space gap out due to SOC, the Berry curvature introduces along the gapped NLs and creates the transverse voltage in the system.^{4,18} If the Weyl points or gapped NLs are near the Fermi level, their signatures can be observed in the anomalous transport properties of materials.^{41,50} For example, the first discovered magnetic WSMs $\text{Co}_3\text{Sn}_2\text{S}_2$ shows the large anomalous Hall conductivity (AHC) due to the gapped NLs and the Weyl points present in the system.⁵⁰ The ANE in the $\text{Co}_3\text{Sn}_2\text{S}_2$, Mn_3X ($\text{X} = \text{Ge}, \text{Sn}$), and Fe_3X ($\text{X} = \text{Ga}, \text{Al}$) is interesting due to their characteristic low-energy electronics structure, including Weyl points near to the Fermi energy.^{21–24} Among the different classes of materials, Heusler alloys are promising for their wide range of properties.^{51–53} Recently, Heusler compounds attracted much interest as quantum material because some of them are discovered as magnetic WSM due to the co-existence of the magnetism and the topology.^{18,40–42,54} Heusler compounds also promise the large AHE and ANE due to large Berry curvature associated with their topological band structure.^{18,55} The largest AHC (~ 1260 ¹⁸ and 2000 S/cm at 2T ⁵⁶) and anomalous Nernst conductivity (ANC) (~ 4 A/m-K⁵⁶) so far reported in the Co_2MnGa magnetic Heusler compound.

The Cu_2CoSn Heusler compound has been identified as the topological semimetal in the topological material database and expected to exhibit large AHC.^{57–59} In the present manuscript, we theoretically investigated the structural, magnetic, and anomalous transport properties in the Cu_2CoSn Heusler compound. Cu_2CoSn is a ferromagnetic material, which exhibits the NLs at the Fermi level, which are protected by the mirror symmetry of the lattice. Upon introducing the SOC in the Hamiltonian and by setting the magnetization axis along the [001] direction, we found that the NLs gapped out and the large Berry curvature appears over the Fermi surface, which results in the large AHC and ANC in the system. The Berry curvature calculation gives the AHC and ANC around ~ 1000 S/cm and ~ 3.98 A/m-K at the Fermi level, which is comparable to the largest reported AHC and ANC in the well-known Co_2MnGa Heusler compound.¹⁸

The *ab initio* calculation for the electronic band structure of Cu_2CoSn was performed by employing the density functional theory using the Quantum Espresso code.⁶⁰ The Plane wave basis set and the Optimized norm-conserving Vanderbilt pseudo-potentials⁶¹ were used for the calculation. The plane wave cutoff energy was chosen at 80 Ry, and the exchange-correlation functional was chosen in the generalized gradient approximation.⁶² The integration in k -space was carried out with $8 \times 8 \times 8$ grid, and the convergence criterion of total

energy was chosen 10^{-8} eV. We extracted the Wannier functions from the DFT bands by Wannier90 code.^{63,64} The maximally localized Wannier functions (MLWFs) for p orbitals on Sn, p_z and d orbitals on Cu, and s, p_z , and d orbitals on Co have been used as the basis of the tight-binding Hamiltonian. The Kubo formula implemented in the Wannier90 code was used for the calculation of the Berry curvature, which can be given as⁶⁵

$$\Omega_{ij}^n = i \sum_{n \neq n'} \frac{\langle n | \frac{\partial H}{\partial R^i} | n' \rangle \langle n' | \frac{\partial H}{\partial R^j} | n \rangle - (i \leftrightarrow j)}{(E_n - E_{n'})^2}. \quad (1)$$

Here, E_n and $|n\rangle$ are the eigenvalue and eigenstate of the Hamiltonian H . The AHC can be calculated using the following equation:

$$\sigma_{ij} = -\frac{e^2}{\hbar} \sum_n \int \frac{d^3k}{(2\pi)^3} \Omega_{ij}^n f_n. \quad (2)$$

Here, f_n represents the Fermi distribution function.

The expression for ANC can be given as¹⁸

$$\alpha_{ij}^A(T, \mu) = -\frac{1}{T} \frac{e}{\hbar} \sum_n \int \frac{d^3k}{(2\pi)^3} \Omega_{ij}^n \left[(E_n - \mu) f_n + K_B T \ln \left(1 + \exp \left(-\frac{E_n - \mu}{K_B T} \right) \right) \right]. \quad (3)$$

Near zero temperature, the above equation can be written as

$$\frac{\alpha_{ij}^A}{T} = -\frac{\pi^2 K_B^2}{3 e} \frac{d\sigma_{ij}}{d\mu}, \quad (4)$$

where α_{ij}^A , K_B , σ_{ij} , and μ are the ANC, Boltzmann constant, AHC, and chemical potential, respectively.

We investigated the Cu_2CoSn regular full Heusler compound with space group $\text{Fm}\bar{3}\text{m}$, and the unit cell of the compound is shown in Fig. 1(a). The special Wyckoff's positions 8c (0.25, 0.25, 0.25), 4b (0.5, 0.5, 0.5), and 4a (0, 0, 0) were considered for Cu, Co, and Sn atoms, respectively. The crystal structure has space inversion symmetry with three perpendicular relevant mirror planes. Figure 1(b) shows the energy vs lattice parameter curve, which suggests the lattice

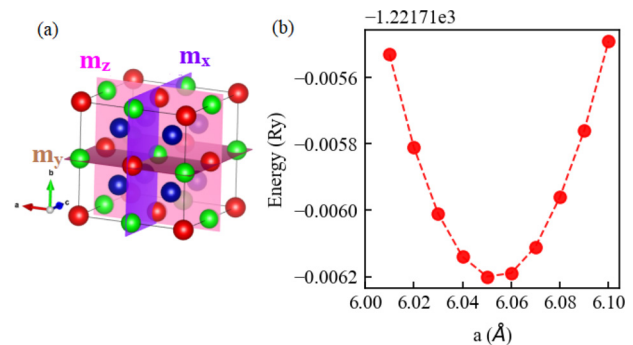


FIG. 1. (a) An unit cell of Cu_2CoSn Heusler compound. Blue, red, and green colors represent the Cu, Co, and Sn atoms, respectively. Three perpendicular mirror planes are designated as m_x , m_y , and m_z , respectively. (b) Energy vs lattice parameter curve for the Cu_2CoSn Heusler compound.

parameter $a = b = c = 6.05 \text{ \AA}$ for the present system. The compound is ferromagnetic with a magnetic moment of $1.15 \mu_B$ per formula of the unit cell. The cobalt atom contributes exclusively to the magnetization ($\mu_{Co} = 1.147 \mu_B/\text{f.u.}$) as Cu and Sn are the non-magnetic elements. The non-integer magnetic moment suggests that the system deviates from the half-metallic behavior. In the absence of SOC, the crystal symmetry of magnetic Cu_2CoSn full Heusler compound belongs to space group $\text{Fm}\bar{3}\text{m}$, which exhibits three relevant mirror reflection symmetries $m_x = 0$, $m_y = 0$, and $m_z = 0$ in the planes $k_x = 0$, $k_y = 0$, and $k_z = 0$, respectively.^{41,66,67} In each of these planes, there is a mirror symmetry protected NL in the Brillouin zone derived from the opposite eigenvalue of mirror symmetries and cross each other at six distinct points.^{42,66,67} These NLs gap out in the presence of SOC according to the magnetization direction, e.g., if the magnetization is considered along the [001] direction, then the mirror symmetries m_x and m_y are no longer remain symmetry planes, while the m_z remains the symmetry plane, as the z -component of the spin S_z is left invariant by m_z . Therefore, the NL in the $k_x = 0$ and $k_y = 0$ planes gap out, while the NL in the $k_z = 0$ remain still protected by the mirror reflection symmetry. The total outward Berry flux from the gapless NL is zero, while the gapped NLs produce the non-zero Berry flux in the surrounding area.^{41,68} The NLs in the $k_x = 0$ and $k_y = 0$ planes gapped out due to SOC result in the band anti-crossings, which restricts the Berry curvature to be aligned in the magnetization direction.⁶⁹

Figure 2(a) represents the Brillouin zone of the FCC lattice with high-symmetry lines and points. The spin-polarized band structure of Cu_2CoSn along high-symmetry k path $X(0.5, 0, 0.5)-\Gamma(0, 0, 0)-L(0.5, 0.5, 0.5)-W(0.5, 0.25, 0.75)-K(0.375, 0.375, 0.750)-\Gamma(0, 0, 0)$ in the $k_z = 0$ plane is shown Fig. 2(b). Noteworthy, the coordinates of high-symmetry point L remain the same regardless of the chosen plane. The red and blue colors represent the majority and minority states, respectively. Two crossings—one is made from the crossing of the majority and minority spin states (say A) and another between minority spin states (say B) at the Fermi level along the $K-\Gamma$ direction [inset

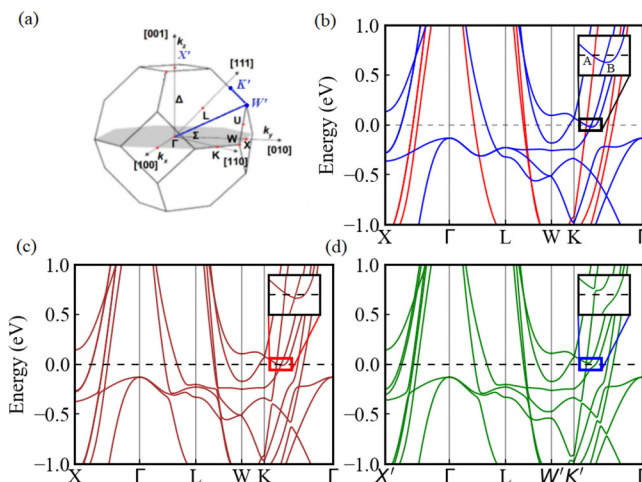


FIG. 2. (a) A Brillouin zone of the face-centered cubic lattice with high-symmetry points and lines. (b) Spin-polarized band structure (spin-up: red; spin-down: blue) in $k_z = 0$ plane. (c) Band structure with spin-orbit coupling (SOC) in the $k_z = 0$ plane. (d) Band structure with SOC in $k_x = 0$ plane. The inset of (b)-(d) shows an enlarged view around the crossing points A and B along the $K-\Gamma$ direction.

of Fig. 2(b)]—seems feature of interest in the band structure as there is a possibility of the formation of NL in the Brillouin zone. Since SOC plays a pivotal role to realize the anomalous transport in materials and is also ubiquitous in materials with 3d elements,⁴¹ it is necessary to study the band structure with non-vanishing SOC. The band structure in the presence of SOC in the $k_z = 0$ plane of the Brillouin zone is shown in Fig. 2(c). The crossing points A and B are still intact with SOC [inset of Fig. 2(c)], which indicates that crossings (NLs) are still protected by the m_z mirror reflection symmetry of the lattice. Now, we plotted the SOC band structure of the Cu_2CoSn along the high-symmetry k path $X'(0, 0.5, 0.5)-\Gamma(0, 0, 0)-L(0.5, 0.5, 0.5)-W'(0.75, 0.25, 0.50)-K'(0.750, 0.375, 0.375)-\Gamma(0, 0, 0)$ in the $k_x = 0$ plane as shown in Fig. 2(d). The degeneracy of crossing point A lost due to SOC in the $k_x = 0$ plane, and, hence, a gap of 7 meV opens at the crossing point because $k_x = 0$ plane no longer remains symmetry of plane when magnetization is along the [001] direction. The crossing point B also no longer persists due to SOC and disappears. The zoom view around the crossing points A and B is shown in the inset of Fig. 2(d). To calculate the topological properties, e.g., Berry curvature, AHC, and ANC, we constructed the MLWF from the Bloch states using Wannier90 code and found a good match between the electronic and Wannier interpolated band structure. The Wannier interpolation is an effective tool to calculate the k -space integrals, which are involved to find out several properties of materials, such as AHC, ANC, spin Hall conductivity, and optical properties.^{63,64,70}

To visualize the NLs in the Brillouin zone, we plotted the bandgaps corresponding to the band crossings A and B in the two-dimension Brillouin zone on two different k -planes. Figure 3(a-i) shows the energy gap of crossing A in the $k_z = 0$ plane, in which mirror symmetry (m_z) is preserved even in the presence of SOC. As a consequence, a closed NL is observed in this plane as shown in the black color, which is protected by the m_z mirror reflection symmetry. The Berry curvature was calculated in the same $k_z = 0$ plane as presented in Fig. 3(a-iii), which shows that the Berry curvature around the preserved NL is very weak. It is interesting to look at the NL and Berry curvature in the $k_x = 0$ plane, which is not a plane of symmetry after considering the SOC and the magnetization direction. The NL, which was preserved in the $k_z = 0$ plane, gapped out in the $k_x = 0$ plane [Fig. 3(a-ii)], because the mirror symmetry in this plane breaks upon considering the SOC and magnetization direction. The Berry curvature distribution in the same $k_x = 0$ planes is shown in Fig. 3(a-iv). As expected, a strong Berry curvature induces along the gapped NL, which can manifest a large transverse response in the system. A similar kind of NL and the Berry curvature is also expected in the $k_y = 0$ plane. Similarly, we have also plotted the energy gap and Berry curvature for crossing B in the $k_z = 0$ and $k_x = 0$ planes as shown in Figs. 3(b-i)–3(b-iv). The closed gap along the $\Gamma-K$ direction (in $k_z = 0$ plane) disappears in the $k_x = 0$ plane, and the Berry curvature appears at the gapped line. Huyen *et al.* studied the AHE in the antiferromagnetic manganese nitrides and found that despite having a lower number of Weyl point around the Fermi level, the AHC is highest in Mn_3PtN due to large Berry curvature at the Fermi surface originated from the high SOC of Pt element.⁷¹ We have also analyzed the Fermi surface of Cu_2CoSn along with the Berry curvature for the present system. Figure 3(c-i) shows the Fermi contours on the mirror plane at $k_z = 0$ with SOC. Along the $\Gamma-X(010)$ direction, we found three Fermi lines out of them two are degenerate (shown inside rectangular

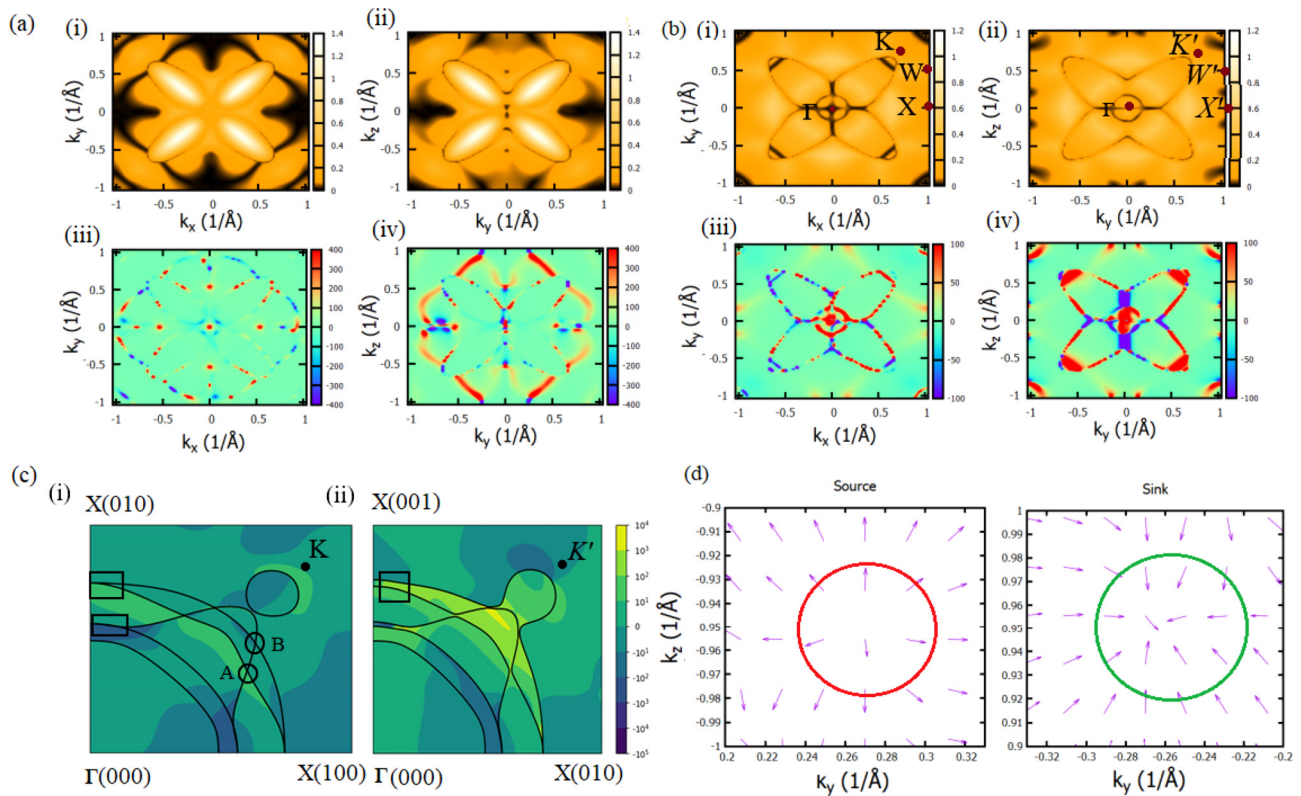


FIG. 3. (a) and (b) The energy gap in (i) $k_z=0$ plane (ii) $k_x=0$ plane and Berry curvature distribution in the (iii) $k_z=0$ plane and (iv) $k_x=0$ plane, for crossings A and B, respectively. The black color in (i) and (ii) represents the vanishing energy gap of the bands. (c) Fermi surface (solid lines) and Berry curvature (color map) in the (i) $k_z=0$ plane and (ii) $k_x=0$ plane. (d) The normalized Berry curvature for the Weyl points in the $k_x=0$ plane. The Weyl points act as the source and drain of the Berry flux.

bracket) and also two Fermi crossings (NLs), which are shown inside the circle. In the Fermi contour on $k_z=0$ plane, the negligible Berry curvature is found to be associated with the Fermi lines. We plotted the same Fermi contour in $k_x=0$ plane with SOC as shown in Fig. 3(c-ii). We observed that at one of the crossing points (crossing A), a tiny gap opens and another Fermi line (crossing B) disappears from the contour due to which a large Berry curvature emerges at the Fermi surface. Also, a small Berry curvature arises from the lifted degeneracy of the bands along the Γ -X(010) direction as shown inside the rectangle of Fig. 3(c-ii). Therefore, the gapped NLs at the Fermi-energy are the main source of the Berry curvature in the system.

Since the mirror symmetry is broken in both $k_y=0$ and $k_x=0$ planes upon considering SOC and [001] magnetization, the Weyl points can only emerge in these planes. The mirror symmetry is still preserved in $k_z=0$ planes; therefore, the Weyl point cannot be in the $k_z=0$ plane. Noteworthy, these Weyl points do not exist in the system naturally due to SOC but rather derived from the NLs, because at some k -points the NLs refuse to break out.^{42,54} The Berry curvature due to Weyl points derived from the gapped NL is typically small as sometimes they lie far away from the Fermi level and/or due to other Weyl points present in the same plane.^{42,54} The energy and momentum space location of the Weyl points due to the breaking of NL in possible k -planes are mentioned in Table I. To further confirm the obtained points as the Weyl points, we plotted the normalized Berry

curvature enclosing the coordinates of the Weyl points in $k_x=0$ plane [Fig. 3(d)]. We found that the Weyl point of chirality +1 acts as a source of Berry curvature [outward flux in Fig. 3(d)] and the Weyl point with chirality -1 acts as a sink of Berry curvature [inward flux in Fig. 3(d)]. The emerging Berry curvature due to the gapped NLs at the Fermi level is supposed to create the large AHC in the material. For this, we calculated the AHC by the integration of Berry curvature of all occupied dispersion bands using Eqs. (1) and (2). In the underlying space group with the magnetization along [001] direction, the Berry curvature pseudo-vector follows the relation:⁷²

$$\begin{aligned}\Omega_x(k_x, k_y, -k_z) &= -\Omega_x(k_x, k_y, k_z), \\ \Omega_y(k_x, k_y, -k_z) &= -\Omega_y(k_x, k_y, k_z), \\ \Omega_z(k_x, k_y, -k_z) &= \Omega_z(k_x, k_y, k_z),\end{aligned}\quad (5)$$

TABLE I. Representative coordinates of Weyl points in different planes in the momentum space with their chemical potentials concerning the Fermi energy.

Weyl point	$k_x (2\pi/a)$	$k_y (2\pi/a)$	$k_z (2\pi/a)$	E (eV)
$W_{\pm A}$	0.26	0.00	± 0.95	-0.240
$W_{\pm B}$	0.00	± 0.26	∓ 0.95	0.235
$W_{\pm C}$	0.00	0.00	± 0.51	0.73

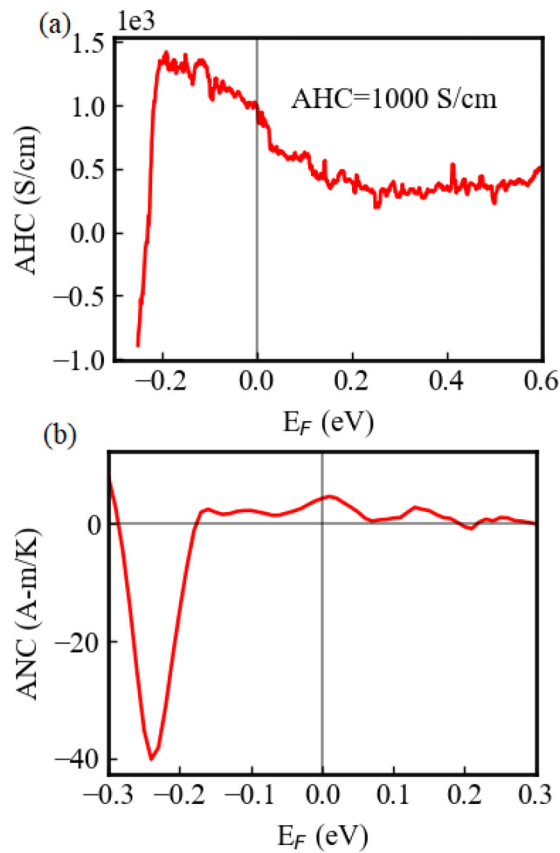


FIG. 4. (a) Fermi-level dependent. (a) Anomalous Hall conductivity. (b) Anomalous Nernst conductivity.

which forces $\Omega_x = \Omega_y = 0$. Therefore, the z-component of AHC σ_z^A is unrestricted, while σ_x^A and σ_y^A identically vanish. The variation of AHC with Fermi energy is shown in Fig. 4(a). We found the giant intrinsic AHC (σ_z^A) about 1003 S/cm at the Fermi energy, which varies to 1120 S/cm just 0.05 eV below the Fermi level. This magnitude of AHC is larger than most of the investigated systems^{19,21,41,73–75} and comparable to the highest AHC reported for Co_2MnGa Heusler compound.^{18,56}

Now we will discuss the ANE in the present compound. The ANE is the thermoelectric counterpart of AHE, where the temperature gradient is used for the motion of charges instead of the electric field.⁷⁶ The origin of ANE is closely related to the AHE, and the key difference is that the AHE is the summation of the Berry curvature over all occupied states, while the ANE is the sum of the Berry curvature of states close to the Fermi energy, i.e., the ANC is the sum of the Berry curvature on the Fermi surface.^{67,76} The magnitude of ANC is related to the variation of the AHC near the Fermi energy. The strong Berry curvature on the Fermi surface gives the $\frac{\partial \sigma_z^A}{\partial E} = 0.013 \text{ A/m K}^2$ and, hence, the ANC reaches the $\sim 3.98 \text{ A/m K}$ at 300 K, which is similar to the highest reported value of ANC that is 4.0 A/m K in the Co_2MnGa experimentally. The variation of the ANC with the Fermi energy is shown in Fig. 4(b).

In conclusion, we theoretically investigated the electronic, magnetic, and anomalous transport properties of Cu_2CoSn full Heusler

compound. We have shown that the gapped NLs at the Fermi energy lead to the large AHC and ANC in the system. Therefore, the Cu_2CoSn is added as a new candidate in the family of Heusler compounds with high AHC and ANC. Our work provides a comprehensive understanding of the anomalous transport properties in the NL hosting magnetic materials and motivates for the further exploration of the Cu_2CoSn Heusler compound through experimental studies.

We gratefully acknowledge the PARAMSHIVAY Supercomputing Centre of IIT(BHU) for cluster support. S.S. thanks the Science and Engineering Research Board of India for financial support through the “CRG” scheme (Grant No. CRG/2021/003256) and UGC-DAE CSR, Indore, for financial support through the “CRS” scheme. G.K.S. thanks the DST-INSPIRE scheme for support through a fellowship.

AUTHOR DECLARATIONS

Conflict of Interest

The authors have no conflicts to disclose.

Author Contributions

Gaurav Kumar Shukla: Conceptualization (lead); Data curation (lead); Formal analysis (lead); Investigation (lead); Writing – original draft (lead). **Ujjawal Modanwal:** Conceptualization (supporting); Formal analysis (supporting). **Sanjay Singh:** Conceptualization (lead); Funding acquisition (lead); Supervision (lead); Writing – review & editing (lead).

DATA AVAILABILITY

The data of the present study are available from the corresponding author upon reasonable request.

REFERENCES

- N. Nagaosa, “Anomalous Hall effect—A new perspective,” *J. Phys. Soc. Jpn.* **75**, 042001 (2006).
- N. Nagaosa, J. Sinova, S. Onoda, A. H. MacDonald, and N. P. Ong, “Anomalous Hall effect,” *Rev. Mod. Phys.* **82**, 1539 (2010).
- D. Yue and X. Jin, “Towards a better understanding of the anomalous Hall effect,” *J. Phys. Soc. Jpn.* **86**, 011006 (2017).
- K. Manna, Y. Sun, L. Muechler, J. Kübler, and C. Felser, “Heusler, Weyl and Berry,” *Nat. Rev. Mater.* **3**, 244 (2018).
- Y. Sakuraba, K. Hyodo, A. Sakuma, and S. Mitani, “Giant anomalous Nernst effect in the $\text{Co}_2\text{MnAl}_{1-x}\text{Si}_x$ Heusler alloy induced by Fermi level tuning and atomic ordering,” *Phys. Rev. B* **101**, 134407 (2020).
- G. K. Shukla, J. Sau, V. Kumar, M. Kumar, and S. Singh, “Band splitting induced Berry flux and intrinsic anomalous Hall conductivity in the NiCoMnGa quaternary Heusler compound,” *Phys. Rev. B* **106**, 045131 (2022).
- N. Shahi, A. K. Jena, G. K. Shukla, V. Kumar, S. Rastogi, K. K. Dubey, I. Rajput, S. Baral, A. Lakhani, S.-C. Lee, S. Bhattacharjee, and S. Singh, “Antisite disorder and Berry curvature driven anomalous Hall effect in the spin gapless semiconducting Mn_2CoAl Heusler compound,” *Phys. Rev. B* **106**, 245137 (2022).
- A. K. Singh, G. K. Shukla, and S. Singh, “Intrinsic anomalous Hall conductivity and real space Berry curvature induced topological Hall effect in Ni_2MnGa magnetic shape memory alloy,” *J. Phys. D* **56**, 044004 (2023).
- K. Wang, Y. Zhang, and G. Xiao, “Anomalous Hall sensors with high sensitivity and stability based on interlayer exchange-coupled magnetic thin films,” *Phys. Rev. Appl.* **13**, 064009 (2020).

- ¹⁰J. Ning, Y. Zhao, Z. Chen, Y. Sun, Q. Gao, Y. Chen, M. Kanagaraj, J. Zhang, and L. He, "Ultra-sensitive anomalous Hall effect sensors based on Cr-doped Bi_2Te_3 topological insulator thin films," *J. Phys. D* **53**, 505001 (2020).
- ¹¹H. Ohno, A. D. Chiba, A. F. Matsukura, T. Omiya, E. Abe, T. Dietl, Y. Ohno, and K. Ohtani, "Electric-field control of ferromagnetism," *Nature* **408**, 944 (2000).
- ¹²J. Smit, "The spontaneous Hall effect in ferromagnetics I," *Physica* **21**, 877 (1955).
- ¹³J. Smit, "The spontaneous Hall effect in ferromagnetics II," *Physica* **24**, 39 (1958).
- ¹⁴R. Karplus and J. Luttinger, "Hall effect in ferromagnetics," *Phys. Rev.* **95**, 1154 (1954).
- ¹⁵G. Sundaram and Q. Niu, "Wave-packet dynamics in slowly perturbed crystals: Gradient corrections and Berry-phase effects," *Phys. Rev. B* **59**, 14915 (1999).
- ¹⁶D. Xiao, M.-C. Chang, and Q. Niu, "Berry phase effects on electronic properties," *Rev. Mod. Phys.* **82**, 1959 (2010).
- ¹⁷M. Ikhlās, T. Tomita, T. Koretsune, M.-T. Suzuki, D. Nishio-Hamane, R. Arita, Y. Otani, and S. Nakatsuji, "Large anomalous Nernst effect at room temperature in a chiral antiferromagnet," *Nat. Phys.* **13**, 1085 (2017).
- ¹⁸S. N. Guin, K. Manna, J. Noky, S. J. Watzman, C. Fu, N. Kumar, W. Schnelle, C. Shekhar, Y. Sun, J. Gooth *et al.*, "Anomalous Nernst effect beyond the magnetization scaling relation in the ferromagnetic Heusler compound Co_2MnGa ," *NPG Asia Mater.* **11**, 16 (2019).
- ¹⁹T. Asaba, V. Ivanov, S. Thomas, S. Savrasov, J. Thompson, E. Bauer, and F. Ronning, "Colossal anomalous Nernst effect in a correlated noncentrosymmetric kagome ferromagnet," *Sci. Adv.* **7**, eabf1467 (2021).
- ²⁰M. Mizuguchi and S. Nakatsuji, "Energy-harvesting materials based on the anomalous Nernst effect," *Sci. Technol. Adv. Mater.* **20**, 262 (2019).
- ²¹T. Chen, S. Minami, A. Sakai, Y. Wang, Z. Feng, T. Nomoto, M. Hirayama, R. Ishii, T. Koretsune, R. Arita *et al.*, "Large anomalous Nernst effect and nodal plane in an iron-based kagome ferromagnet," *Sci. Adv.* **8**, eabk1480 (2022).
- ²²A. Sakai, S. Minami, T. Koretsune, T. Chen, T. Higo, Y. Wang, T. Nomoto, M. Hirayama, S. Miwa, D. Nishio-Hamane *et al.*, "Iron-based binary ferromagnets for transverse thermoelectric conversion," *Nature* **581**, 53 (2020).
- ²³H. Yang, W. You, J. Wang, J. Huang, C. Xi, X. Xu, C. Cao, M. Tian, Z.-A. Xu, J. Dai, and Y. Li, "Giant anomalous Nernst effect in the magnetic Weyl semimetal $\text{Co}_3\text{Sn}_2\text{S}_2$," *Phys. Rev. Mater.* **4**, 024202 (2020).
- ²⁴G.-Y. Guo and T.-C. Wang, "Large anomalous Nernst and spin Nernst effects in the noncollinear antiferromagnets Mn_3X (X = Sn, Ge, Ga)," *Phys. Rev. B* **96**, 224415 (2017).
- ²⁵S. Wang, B.-C. Lin, A.-Q. Wang, D.-P. Yu, and Z.-M. Liao, "Quantum transport in Dirac and Weyl semimetals: A review," *Adv. Phys. X* **2**, 518 (2017).
- ²⁶M. Z. Hasan, G. Chang, I. Belopolski, G. Bian, S.-Y. Xu, and J.-X. Yin, "Weyl, Dirac and high-fold chiral fermions in topological quantum matter," *Nat. Rev. Mater.* **6**, 784 (2021).
- ²⁷A. H. Castro Neto, F. Guinea, N. M. R. Peres, K. S. Novoselov, and A. K. Geim, "The electronic properties of graphene," *Rev. Mod. Phys.* **81**, 109 (2009).
- ²⁸M. Z. Hasan and C. L. Kane, "Colloquium: Topological insulators," *Rev. Mod. Phys.* **82**, 3045 (2010).
- ²⁹O. Vafek and A. Vishwanath, "Dirac fermions in solids: From high- T_c cuprates and graphene to topological insulators and Weyl semimetals," *Annu. Rev. Condens. Matter Phys.* **5**, 83 (2014).
- ³⁰H. Weyl, *Gesammelte Abhandlungen: Band 1 Bis 4* (Springer-Verlag, 1968), Vol. 4.
- ³¹A. Burkov, "Topological semimetals," *Nat. Mater.* **15**, 1145 (2016).
- ³²M. Z. Hasan, S.-Y. Xu, I. Belopolski, and S.-M. Huang, "Discovery of Weyl fermion semimetals and topological Fermi arc states," *Annu. Rev. Condens. Matter Phys.* **8**, 289 (2017).
- ³³N. P. Armitage, E. J. Mele, and A. Vishwanath, "Weyl and Dirac semimetals in three-dimensional solids," *Rev. Mod. Phys.* **90**, 015001 (2018).
- ³⁴B. Yan and C. Felser, "Topological materials: Weyl semimetals," *Annu. Rev. Condens. Matter Phys.* **8**, 337 (2017).
- ³⁵S.-Y. Xu, I. Belopolski, N. Alidoust, M. Neupane, G. Bian, C. Zhang, R. Sankar, G. Chang, Z. Yuan, C.-C. Lee *et al.*, "Discovery of a Weyl Fermion semimetal and topological Fermi arcs," *Science* **349**, 613 (2015).
- ³⁶L. Yang, Z. Liu, Y. Sun, H. Peng, H. Yang, T. Zhang, B. Zhou, Y. Zhang, Y. Guo, M. Rahn *et al.*, "Weyl semimetal phase in the non-centrosymmetric compound TaAs," *Nat. Phys.* **11**, 728 (2015).
- ³⁷B. Lv, N. Xu, H. Weng, J. Ma, P. Richard, X. Huang, L. Zhao, G. Chen, C. Matt, F. Bisti *et al.*, "Observation of Weyl nodes in TaAs," *Nat. Phys.* **11**, 724 (2015).
- ³⁸Y. Sun, Y. Zhang, C. Felser, and B. Yan, "Strong intrinsic spin Hall effect in the TaAs family of Weyl semimetals," *Phys. Rev. Lett.* **117**, 146403 (2016).
- ³⁹S.-Y. Xu, I. Belopolski, D. S. Sanchez, C. Zhang, G. Chang, C. Guo, G. Bian, Z. Yuan, H. Lu, T.-R. Chang *et al.*, "Experimental discovery of a topological Weyl semimetal state in TaP," *Sci. Adv.* **1**, e1501092 (2015).
- ⁴⁰P. Chaudhary, K. K. Dubey, G. K. Shukla, S. Singh, S. Sadhukhan, S. Kanungo, A. K. Jena, S.-C. Lee, S. Bhattacharjee, J. Minár, and S. W. D'Souza, "Role of chemical disorder in tuning the Weyl points in Vanadium doped Co_2TiSn ," *Phys. Rev. Mater.* **5**, 124201 (2021).
- ⁴¹G. K. Shukla, J. Sau, N. Shahi, A. K. Singh, M. Kumar, and S. Singh, "Anomalous Hall effect from gapped nodal line in the Co_2FeGe Heusler compound," *Phys. Rev. B* **104**, 195108 (2021).
- ⁴²Z. Wang, M. G. Vergniory, S. Kushwaha, M. Hirschberger, E. V. Chulkov, A. Ernst, N. P. Ong, R. J. Cava, and B. A. Bernevig, "Time-reversal-breaking Weyl fermions in magnetic Heusler alloys," *Phys. Rev. Lett.* **117**, 236401 (2016).
- ⁴³A. Burkov, M. Hook, and L. Balents, "Topological nodal semimetals," *Phys. Rev. B* **84**, 235126 (2011).
- ⁴⁴M. Phillips and V. Aji, "Tunable line node semimetals," *Phys. Rev. B* **90**, 115111 (2014).
- ⁴⁵C. Fang, Y. Chen, H.-Y. Kee, and L. Fu, "Topological nodal line semimetals with and without spin-orbital coupling," *Phys. Rev. B* **92**, 081201 (2015).
- ⁴⁶Y. Kim, B. J. Wieder, C. L. Kane, and A. M. Rappe, "Dirac line nodes in inversion-symmetric crystals," *Phys. Rev. Lett.* **115**, 036806 (2015).
- ⁴⁷G. Bian, T.-R. Chang, R. Sankar, S.-Y. Xu, H. Zheng, T. Neupert, C.-K. Chiu, S.-M. Huang, G. Chang, I. Belopolski *et al.*, "Topological nodal-line fermions in spin-orbit metal PbTaSe_2 ," *Nat. Commun.* **7**, 10556 (2016).
- ⁴⁸L. M. Schoop, M. N. Ali, C. Straßer, A. Topp, A. Varykhalov, D. Marchenko, V. Duppel, S. S. Parkin, B. V. Lotsch, and C. R. Ast, "Dirac cone protected by non-symmorphic symmetry and three-dimensional Dirac line node in ZrSiS ," *Nat. Commun.* **7**, 11696 (2016).
- ⁴⁹J. Hu, Z. Tang, J. Liu, X. Liu, Y. Zhu, D. Graf, K. Myhro, S. Tran, C. N. Lau, J. Wei, and Z. Mao, "Evidence of topological nodal-line fermions in ZrSiSe and ZrSiTe ," *Phys. Rev. Lett.* **117**, 016602 (2016).
- ⁵⁰E. Liu, Y. Sun, N. Kumar, L. Muechler, A. Sun, L. Jiao, S.-Y. Yang, D. Liu, A. Liang, Q. Xu *et al.*, "Giant anomalous Hall effect in a ferromagnetic kagome-lattice semimetal," *Nat. Phys.* **14**, 1125 (2018).
- ⁵¹T. Graf, C. Felser, and S. S. Parkin, "Simple rules for the understanding of Heusler compounds," *Prog. Solid State Chem.* **39**(1), 1–50 (2011).
- ⁵²C. Felser, L. Wollmann, S. Chadov, G. H. Fecher, and S. S. Parkin, "Basics and prospective of magnetic Heusler compounds," *APL Mater.* **3**, 041518 (2015).
- ⁵³C. Felser and A. Hirohata, *Heusler Alloys* (Springer, 2015).
- ⁵⁴G. Chang, S.-Y. Xu, H. Zheng, B. Singh, C.-H. Hsu, G. Bian, N. Alidoust, I. Belopolski, D. S. Sanchez, S. Zhang *et al.*, "Room-temperature magnetic topological Weyl fermion and nodal line semimetal states in half-metallic Heusler Co_2TiX (X = Si, Ge, or Sn)," *Sci. Rep.* **6**, 38839 (2016).
- ⁵⁵P. Li, J. Koo, W. Ning, J. Li, L. Miao, L. Min, Y. Zhu, Y. Wang, N. Alem, C.-X. Liu *et al.*, "Giant room temperature anomalous Hall effect and tunable topology in a ferromagnetic topological semimetal Co_2MnAl ," *Nat. Commun.* **11**, 3476 (2020).
- ⁵⁶A. Sakai, Y. P. Mizuta, A. A. Nugroho, R. Sihombing, T. Koretsune, M.-T. Suzuki, N. Takemori, R. Ishii, D. Nishio-Hamane, R. Arita *et al.*, "Giant anomalous Nernst effect and quantum-critical scaling in a ferromagnetic semimetal," *Nat. Phys.* **14**, 1119 (2018).
- ⁵⁷B. Bradlyn, L. Elcoro, J. Cano, M. Vergniory, Z. Wang, C. Felser, M. I. Aroyo, and B. A. Bernevig, "Topological quantum chemistry," *Nature* **547**, 298 (2017).
- ⁵⁸M. Vergniory, L. Elcoro, C. Felser, N. Regnault, B. A. Bernevig, and Z. Wang, "A complete catalogue of high-quality topological materials," *Nature* **566**, 480 (2019).
- ⁵⁹Y. Ji, W. Zhang, H. Zhang, and W. Zhang, "Spin Hall conductivity and anomalous Hall conductivity in full Heusler compounds," *New J. Phys.* **24**, 053027 (2022).
- ⁶⁰P. Giannozzi, S. Baroni, N. Bonini, M. Calandra, R. Car, C. Cavazzoni, D. Ceresoli, G. L. Chiarotti, M. Cococcioni, I. Dabo, A. D. Corso, S. de Gironcoli, S. Fabris, G. Fratesi, R. Gebauer, U. Gerstmann, C. Gougoussis, A. Kokalj, M. Lazzeri, L. Martin-Samos, N. Marzari, F. Mauri, R. Mazzarello, S. Paolini,

- A. Pasquarello, L. Paulatto, C. Sbraccia, S. Scandolo, G. Sclauzero, A. P. Seitsonen, A. Smogunov, P. Umari, and R. M. Wentzcovitch, "QUANTUM ESPRESSO: A modular and open-source software project for quantum simulations of materials," *J. Phys. Condens. Matter* **21**, 395502 (2009).
- ⁶¹D. R. Hamann, "Optimized norm-conserving vanderbilt pseudopotentials," *Phys. Rev. B* **88**, 085117 (2013).
- ⁶²J. P. Perdew, K. Burke, and M. Ernzerhof, "Generalized gradient approximation made simple," *Phys. Rev. Lett.* **77**, 3865 (1996).
- ⁶³N. Marzari and D. Vanderbilt, "Maximally localized generalized Wannier functions for composite energy bands," *Phys. Rev. B* **56**, 12847 (1997).
- ⁶⁴I. Souza, N. Marzari, and D. Vanderbilt, "Maximally localized Wannier functions for entangled energy bands," *Phys. Rev. B* **65**, 035109 (2001).
- ⁶⁵M. Gradhand, D. V. Fedorov, F. Pientka, P. Zahn, I. Mertig, and B. L. Györfly, *J. Phys.: Condens. Matter* **24**, 213202 (2012).
- ⁶⁶J. Noky, Q. Xu, C. Felser, and Y. Sun, "Large anomalous Hall and Nernst effects from nodal line symmetry breaking in Fe_2MnX ($X = \text{P}, \text{As}, \text{Sb}$)," *Phys. Rev. B* **99**, 165117 (2019).
- ⁶⁷J. Noky, J. Gooth, C. Felser, and Y. Sun, "Characterization of topological band structures away from the Fermi level by the anomalous Nernst effect," *Phys. Rev. B* **98**, 241106 (2018).
- ⁶⁸B. Ernst, R. Sahoo, Y. Sun, J. Nayak, L. Muechler, A. K. Nayak, N. Kumar, J. Gayles, A. Markou, G. H. Fecher, and C. Felser, "Anomalous Hall effect and the role of Berry curvature in Co_2TiSn Heusler films," *Phys. Rev. B* **100**, 054445 (2019).
- ⁶⁹K. Manna, L. Muechler, T.-H. Kao, R. Stinshoff, Y. Zhang, J. Gooth, N. Kumar, G. Kreiner, K. Koepf, R. Car, J. Kübler, G. H. Fecher, C. Shekhar, Y. Sun, and C. Felser, "From colossal to zero: Controlling the anomalous Hall effect in magnetic Heusler compounds via Berry curvature design," *Phys. Rev. X* **8**, 041045 (2018).
- ⁷⁰G. K. Shukla, A. K. Jena, N. Shahi, K. K. Dubey, I. Rajput, S. Baral, K. Yadav, K. Mukherjee, A. Lakhani, K. Carva, S.-C. Lee, S. Bhattacharjee, and S. Singh, "Atomic disorder and Berry phase driven anomalous Hall effect in a Co_2FeAl Heusler compound," *Phys. Rev. B* **105**, 035124 (2022).
- ⁷¹V. T. N. Huyen, M.-t Suzuki, K. Yamauchi, and T. Oguchi, "Topology analysis for anomalous Hall effect in the noncollinear antiferromagnetic states of Mn_3AN ($A = \text{Ni}, \text{Cu}, \text{Zn}, \text{Ga}, \text{Ge}, \text{Pd}, \text{In}, \text{Sn}, \text{Ir}, \text{Pt}$)," *Phys. Rev. B* **100**, 094426 (2019).
- ⁷²I. Samathrakris, N. Fortunato, H. K. Singh, C. Shen, and H. Zhang, "Tunable anomalous Hall and Nernst effects in MMX compounds," [arXiv:2207.03320](https://arxiv.org/abs/2207.03320) (2022).
- ⁷³F. Mende, J. Noky, S. N. Guin, G. H. Fecher, K. Manna, P. Adler, W. Schnelle, Y. Sun, C. Fu, and C. Felser, "Large anomalous Hall and Nernst effects in high Curie-temperature iron-based Heusler compounds," *Adv. Sci.* **8**, 2100782 (2021).
- ⁷⁴T. Chen, T. Tomita, S. Minami, M. Fu, T. Koretsune, M. Kitatani, I. Muhammad, D. Nishio-Hamane, R. Ishii, F. Ishii *et al.*, "Anomalous transport due to Weyl fermions in the chiral antiferromagnets Mn_3X , $\text{X} = \text{Sn}, \text{Ge}$," *Nat. Commun.* **12**, 572 (2021).
- ⁷⁵Y. Wang, C. Xian, J. Wang, B. Liu, L. Ling, L. Zhang, L. Cao, Z. Qu, and Y. Xiong, "Anisotropic anomalous Hall effect in triangular itinerant ferromagnet Fe_3GeTe_2 ," *Phys. Rev. B* **96**, 134428 (2017).
- ⁷⁶M. Park, G. Han, and S. H. Rhim, "Anomalous Hall effect in a compensated ferrimagnet: Symmetry analysis for Mn_3Al ," *Phys. Rev. Res.* **4**, 013215 (2022).